

# Energy Estimation as Earthquake Precursor, Using the Energy of the Radiated Particles with the Help of Monte Carlo Methods

Abouzar Bahari\*, Saeed Mohammadi

*Department of Physics, Payame Noor University, Tehran, Iran*

\*Corresponding author, Email: [aboozar.bahari@gmail.com](mailto:aboozar.bahari@gmail.com) , Tel: +989153073257

## Abstract

Scientists have observed variations in the Earth's electromagnetic fields and radiation of some particles like low or high-energy photons, neutrons, protons, etc before, during, and after earthquakes, leading to the hypothesis that changes in particles' energy and flux signals could potentially serve as precursors to seismic activity. In this study, utilizing the relationships between the energy of atomic/nuclear particles released from underground piezoelectric rocks and the elastic energy, stored in these rocks, we introduced some methods to estimate the time/energy of incoming earthquakes in aseismic regions by measuring the energy of radiated particles. Since piezoelectric granite rocks make up approximately 60% of the Earth's crust, the increase in the energy of the detected particles in a certain period of time can be considered as an important precursor for the impending shallow earthquake. This analysis holds significant promise for enhancing earthquake time and energy estimation methodologies. The detection of radiated particles from piezoelectric rocks can be achieved by utilizing detectors placed either on the surface or inside deep wells that are drilled near active faults. However, it is essential to note that the methodologies presented are approximations, as they rely on constant parameters for the piezoelectric material and presuppose that earthquakes occur within a piezoelectric block.

**Keywords:** Earthquake prediction; particle radiation; Granite Rocks; MCNPX; Piezoelectricity

## 1. Introduction

Scientists have observed variations in the Earth's electromagnetic fields and radiation of some particles like low or high-energy photons, neutrons, protons, etc before, during, and after earthquakes, leading to the hypothesis that changes in particles' energy and flux signals could potentially serve as precursors to seismic activity. These anomalies could be detected using magnetometers, electric field sensors, nuclear particle

31 detectors, and other monitoring devices. Researchers are investigating whether monitoring these signals  
32 could provide valuable insights into the build-up of stress along fault lines and the potential for an  
33 impending earthquake.

34 In some parts of the world, earthquakes are often accompanied by lightning. Finkelstein and Powell (1970)  
35 suggested that the piezoelectric effect in the Earth's crust causes the electrical field. In rock with a mean  
36 piezoelectric coefficient, several percent that of x cut single crystal quartz, and with typical seismic stress  
37 changes 30–300 bars, an earthquake makes an average electrical field of 500–5,000 V cm<sup>-1</sup>. For distances  
38 of half the seismic wavelength, the generated voltage is  $5 \times 10^7$  to  $5 \times 10^8$  V, comparable with the voltage  
39 responsible for lightning in storms (Finkelstein and Powell (1970)).

40 The study of Mansouri Daneshvar & Freund (2019) affirms a process, by which tectonic stresses deep in  
41 the Earth's crust lead to positive charges at the surface-to-air interface and air ionization, which can trigger  
42 atmospheric blocks. Fu et al. (2015) identified abnormal changes in gamma-ray counting rates leading up  
43 to localized earthquakes in eastern Taiwan. Maksudov et al. (2017) introduced a novel forecasting approach  
44 based on simultaneous monitoring of low-energy neutron and charged particle flux intensities through  
45 detectors. Volodichev et al. (2000) documented heightened neutron emissions in seismic zones of the Pamir  
46 region, exceeding typical levels by up to two orders of magnitude, particularly before significant  
47 earthquakes of magnitude 4 or greater on the Richter scale.

48 Sigaeva et al. (2006) observed neutron emissions preceding the December 2004 Sumatra earthquake. Borla  
49 et al. (2015) observed a strong correlation among acoustic, EM, and neutron emissions with major  
50 earthquakes in the vicinity of Testa Grigia Laboratory and the Val Trebbia seismic region in Italy. They  
51 noted a noteworthy increase in neutron dose rates, around six times greater than the natural background,  
52 and detected anomalous high-energy neutron components, particularly around 8 MeV, during seismic  
53 activity in granitic areas, thus reinforcing the piezo-nuclear hypothesis.

54 Bahari et al. (2022) employed piezoelectricity principles and elastic energy formulas along with the  
55 MCNPX simulation code to investigate the generation of atomic/nuclear particles, predominant  
56 interactions, and potential particle energies in quartz and granite blocks under mechanical stress. They  
57 demonstrated that in large granite blocks, nuclear particle creation is primarily driven by photonuclear  
58 interactions resulting from Bremsstrahlung gamma-ray photons due to runaway electron avalanches under  
59 stress conditions. Furthermore, they presented formulas to estimate the quantity and energies of various  
60 particles generated on a surface when a piezoelectric block is subjected to varying uniaxial stresses.

61 Bahari et al. (2024) also highlighted the estimation of particle flux from under-stressed granitic rocks using  
62 the MCNPX code at different distances from the earthquake hypocenter inside the fractures filled with air,

63 water, and CO<sub>2</sub>. The study reveals that gases like air and CO<sub>2</sub> can facilitate particle flux far from the seismic  
64 source, with potential detection on the surface. Especially for deep earthquakes, the vacuum-filled fractures  
65 can facilitate the radiated nuclear particles to reach the surface.

66 In addition, Bahari & Mohammadi (2024) simulated the nuclear interactions between the created neutrons  
67 from under-stressed piezoelectric rocks and the elements of granite plus the elements of fractures' filling  
68 fluids. The results indicate that compound nuclear reactions like fusion/ fission/ inelastic scattering can  
69 happen, resulting in the release of energy from the depths of the Earth in the aseismic regions. Furthermore,  
70 compound nuclear interactions from the piezoelectric effect can generate some stable isotopes like  
71 deuterium (<sup>2</sup>H), carbon (C), or oxygen (O) and also some radioisotopes in the granitic rock texture or inside  
72 the fracture-filling fluids. Hence, their study illustrates that an increase in the amount of deuterium or CO<sub>2</sub>  
73 in the water/ air of an aseismic region would be two important precursors of incoming earthquakes.

74 In this study, we aim to leverage the established relationships between accumulated elastic energy and the  
75 energy of radiated particles from piezoelectric rocks under mechanical stress to calculate the rate of elastic  
76 energy accumulation in rocks and faults. This analysis holds significant promise for enhancing earthquake  
77 time and energy estimation methodologies.

78 It is worth mentioning that the detection of radiated particles from piezoelectric rocks can be achieved by  
79 utilizing detectors placed either on the surface or inside deep wells that are drilled near active faults.

80 One might wonder how we can distinguish between piezo atomic/nuclear particles and geo-particles, which  
81 are produced by natural radioactivity. The answer lies in the fact that in a region without seismic activity,  
82 there exists a relatively constant level of detected geo-particles (such as geo-neutrons), known as the  
83 background level. However, when mechanical stress is stored in the rock, the phenomenon of  
84 piezoelectricity leads to an increased flux of particles compared to the background level. Furthermore, the  
85 energy of the detected piezo-particles rises with an increase in mechanical force, whereas geo-particles  
86 generally possess lower average energy. This distinction allows us to discriminate between the two types  
87 of particles.

88 Another question arises regarding the amount of data acquisition time required with existing radiation  
89 detectors to obtain a signal that can be distinguished from background radiation signals. The answer lies in  
90 the fact that as energy accumulates in the underground piezoelectric rock, lower-energy atomic particles  
91 such as electrons or photons are emitted. As the energy accumulation increases, nuclear particles, along  
92 with higher-energy atomic particles, are also emitted. Therefore, the detection of neutrons and high-energy  
93 gamma rays serves as a precursor to strong earthquakes [Bahari et al. (2022)]. Furthermore, it is crucial to  
94 emphasize the significance of time in the early warning of an earthquake. Our previous study using MCNPX

95 simulation revealed that in a 2-kilometer deep air-filled vertical fracture when the source particles are  
 96 neutrons with an energy of 24.6 MeV (Mega electron Volt) and travel from the bottom to the top surface  
 97 of the fracture, the average time for the capture or escape of created photon particles is 1.87E-04 s.  
 98 Additionally, their mean free path (*mfp*) is calculated to be 1.58E+04 cm [Bahari et al. (2024)]. Hence, once  
 99 these particles are generated, they can be promptly accessed and identified, which could aid in providing  
 100 early alerts for approaching earthquakes.

101

## 102 2. Materials and Methods

### 103 2.1. The mechanism of earthquake energy accumulation and its release

104 The process of earthquake energy accumulation and subsequent release involves the sudden transformation  
 105 of stored elastic energy ( $E_{el}$ ) from tectonic forces into kinetic energy ( $E_K$ ) during rock sliding, along with  
 106 residual potential energy after sliding stops ( $E_r$ ) and energy dissipated ( $E_d$ ) through friction and other  
 107 processes [Kunquan et al. (2018)]. This relationship can be expressed as:

$$108 \quad E_{el} = E_K + E_r + E_d \quad (1)$$

109 The acoustic wave energy ( $E_{AC}$ ) responsible for seismic damage originates from the kinetic energy of rock  
 110 sliding. Assuming all potential energy is released, the residual energy ( $E_r$ ) becomes zero. By substituting  
 111  $E_K$  with  $E_{AC}$ , we get:

$$112 \quad E_{el} = E_K + E_d = E_{AC} + E_d \quad (2)$$

113 The dissipated energy ( $E_d$ ) comprises dissipated heat ( $Q$ ), fracture energy ( $E_F$ ), and particle radiation  
 114 ( $E_{radiation}$ ) released from rocks as a result of the piezoelectricity or other mechanisms. Therefore:

$$115 \quad E_d = Q + E_F + E_{radiation} \rightarrow E_{el} = E_{AC} + E_F + E_{radiation} + Q \quad (3)$$

116 Gutenberg and Richter (1956) established a correlation between earthquake energy radiated in elastic waves  
 117 in ergs ( $10^{-7}$  J) and the Richter scale magnitude ( $M_L$ ) of the earthquake:

$$118 \quad \text{Log } E_{AC} = 2.4 m + 5.8 \quad (4)$$

$$119 \quad m = 1.7 + 0.8M_L - 0.01M_L^2$$

120 To determine the elastic energy stored in a rock block under mechanical load, we can simplify the  
 121 calculation by assuming the block is experiencing uniaxial compressive stress ( $\sigma_2 = \sigma_3 = 0$  and  $\sigma_1 = \sigma$ ).

122 The input elastic energy ( $E_{el}$ ) per unit volume of rock in  $\text{J/m}^3$  can be calculated using the following equation  
 123 [Liang et al. (2015) and Gao et al. (2020)]:

124  $E_{el} \text{ per unit volume} = \frac{1}{2} \sigma \varepsilon_{el} = \frac{1}{2} \frac{\sigma^2}{\check{E}}$  (5)

125 where  $\varepsilon_{el}$  represents the elastic strain and  $\check{E}$  is the elasticity modulus in GPa. The total input elastic energy  
 126 in joules can then be determined by:

127  $E_{el} = \frac{1}{2} \frac{\sigma^2}{\check{E}} \mathbb{V}$  (6)

128 with  $\mathbb{V}$  representing the rock volume in  $\text{m}^3$ .

129 **Table 1** provides information on the elastic energy released and the corresponding Richter scale of an  
 130 earthquake for 3 different cubic block sizes of granite, subjected to uniaxial stress at a rupture point of  
 131 approximately 140 MPa and an elastic modulus of 40 GPa, assuming  $E_{el} = E_{Al}$  (no residual or dissipated  
 132 energy) [Bahari et al. (2022)].

133

134 **Table 1:** Elastic energy released and the corresponding Richter scale of an earthquake for 3 different cubic  
 135 block sizes of granite, subjected to uniaxial stress at a rupture point [Bahari et al. (2022)].

Length, m	$\mathbb{V}$ , $\text{m}^3$	$E_{el}$ at rupture point, erg	$M_L$
40	6.4E+4	1.57E+17	4.011
400	6.4E+7	1.57E+20	5.791
4000	6.4E+10	1.57E+23	7.670

136

137 It is important to consider that approximately 60% of the Earth's crust is composed of Granitic rocks.

138

139 **2.2. Correlations between the energies of the radiated particles and the mechanical load applied on a**  
 140 **piezoelectric block**

141 In our prior research, we identified some relationships for the energy of atomic/nuclear particles, generated  
 142 from piezoelectric blocks under stress using MCNPX (Monte Carlo N particles- extended) simulation which  
 143 is a nuclear physics code to simulate the particle's radiations (their energies and paths) through a material  
 144 medium with three-dimensional geometry and continuous-energy transport. Some of these particles may  
 145 travel into empty fractures while maintaining their initial energy until they are detected by near-logging  
 146 tools located in deep wells or surface detectors. The equations representing these relationships are as  
 147 follows [Bahari et al. (2022)]:

148  $The \text{ average energy of created electrons, } MeV = 0.0051 \ln(E_e) + 0.0019$  (7)

149  $The \text{ average energy of created photons, } MeV = 0.5193 \ln(E_e) - 1.6838$  (8)

150 *The average energy of created neutrons, MeV = 4.4984 ln( $E_e$ ) – 17.574* (9)

151 *The average energy of created protons, MeV = 2.4733 ln( $E_e$ ) – 4.1223* (10)

152 In which the piezoelectric relations are [Moheimani and Fleming (2006), Halliday and Resnick (1974)]:

153 
$$E_e = \frac{U_p}{n_e}$$
 (11)

154 
$$U_p = V q$$
 (12)

155 
$$n_e = \frac{q}{e}$$
 (13)

156 
$$q = d F$$
 (14)

157 
$$V = \frac{q}{C_p} = \frac{d F}{C_p} = \frac{d F x}{\epsilon_0 \epsilon_r A}$$
 (15)

158 Where,

159  $E_e$ : the potential energy of each electron, eV,

160  $U_p$ : electric potential energy, J or eV,

161  $V$ : electric voltage, V,

162  $q$ : electric charge, C,

163  $C_p$ : the capacitance of the piezoelectric material, Farad,

164  $n_e$ : number of electrons on the negative charge surface,

165  $e$ : charge of an electron =  $1.602 \times 10^{-19}$  C,

166  $d$ : matrix of piezoelectric coefficients, m/V or C/N,

167  $F$ : applied force on the surfaces, N,

168  $x$ : thickness of the piezoelectric material, m,

169  $\epsilon_0$ : vacuum permittivity =  $8.85 \times 10^{-12}$  F/m = C<sup>2</sup>/N/m<sup>2</sup>,

170  $\epsilon_r$ : relative permittivity (dielectric constant), ( $\epsilon = \epsilon_0 \epsilon_r$ ),

171 According to Eqs. 7-10, once the energy of the particles being detected is determined, it becomes feasible  
 172 to calculate the initial energy of the electrons ( $E_e$ ) in the piezoelectric rocks under stress, along with their  
 173 voltage. Subsequently, an estimation of the mechanical energy stored within the rock and the potential  
 174 magnitude of an earthquake could be derived.

175 It must be taken into account that various particle detectors may apply different methods for particle  
 176 detection. For instance, many photodetectors can be configured to detect individual photons, each with  
 177 relative advantages and disadvantages. Common types include photomultipliers, Geiger counters, single-

178 photon avalanche diodes, superconducting nanowire single-photon detectors, transition edge sensors,  
179 and scintillation counters (Hadfield (2009) and NIST (2013)).

180

### 181 3. Results and discussions

182 To forecast the occurrence of earthquakes, one can utilize Eqs. 7-10. To illustrate this, let us provide an  
183 example. Let's assume that the surface or downhole particle detectors in a seismically stable area record the  
184 average energy of the detected photons. Table 2 presents the assumed average energy of these photons  
185 based on the recording time. Furthermore, it is reasonable to assume that the energy of the emitted photons  
186 increases over time due to the gradual accumulation of elastic energy within the block or fault.

187

188 **Table 2.** Assumed average energy of detected photons, based on the recording time

Recording time, days	Detected photons' average energy, MeV
1	0.0001
10	0.001
100	0.01
200	0.1
350	0.2
500	0.4
700	0.5

189

190 Based on the quantities provided in Table 2, the initial energy of the electrons ( $E_e$ ) and the resulting voltage  
191 ( $V$ ) can be calculated using Eq. 10 and Eqs. 11-15, respectively. By applying Eq. 15, the amount of applied  
192 force ( $F$ ) can be estimated, assuming a constant size ( $x$ ) for the piezoelectric cube. Subsequently, the  
193 uniaxial compressive stress ( $\sigma_z = F_z/x^2$ ) on the block can be computed. Finally, Eq. 6 can be used to  
194 evaluate the accumulated elastic energy ( $E_{el}$ ) and the equivalent Richter magnitude ( $M_L$ ) of the earthquake.

195 In Table 3, the computed piezoelectric and elastic energy parameters, along with the Richter magnitude  
196 ( $M_L$ ), are presented for the incoming earthquake. These calculations are based on the assumed average  
197 energy of the detected photons, as provided in Table 2. The granite block used in the analysis has each side  
198 measuring 40 m. The piezoelectric coefficient is  $7 \times 10^{-13}$  C/N [Matsuda et al. (2005)], the dielectric constant  
199 ( $\epsilon_r$ ) is 5 [Hubbard et al. (1997)], the uniaxial compressive strength is 140 MPa, and the elastic modulus is  
200 40 GPa.

201 It is important to recognize that the piezoelectric coefficient of rocks diminishes with increasing depth,  
202 attributed to the elevated temperatures found in the deeper crust. Hence, the quartz minerals present in

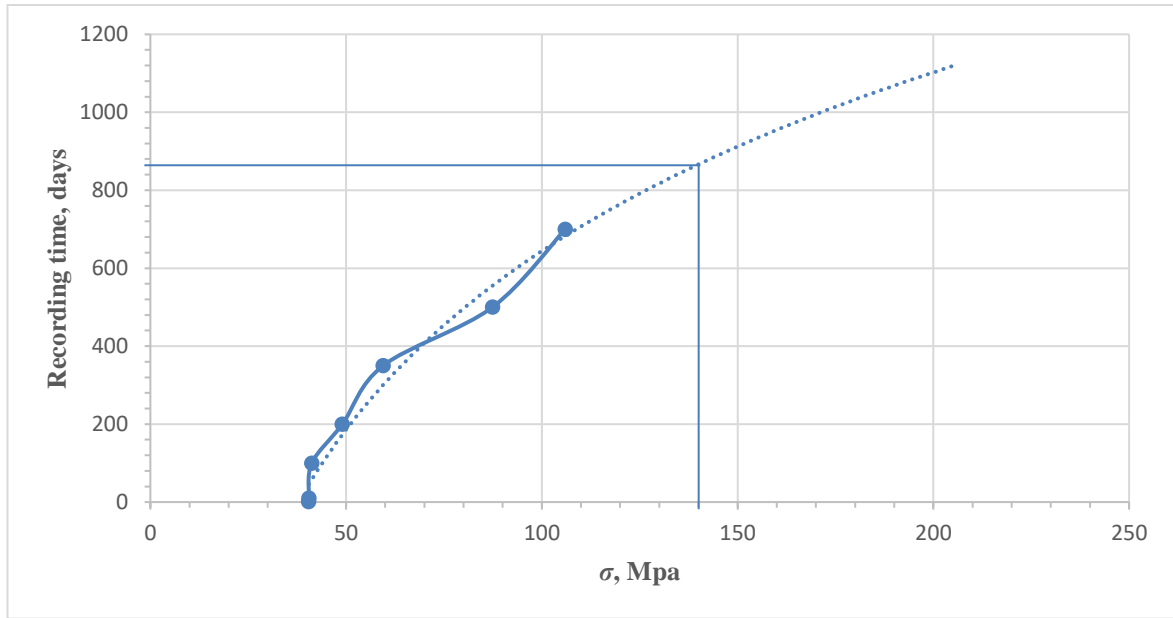
203 granite exhibit the piezoelectric effect at depths reaching up to 23 kilometers (Bahari et al. (2022)). For the  
 204 sake of simplicity, we have assumed that the piezoelectric coefficient remains constant across varying  
 205 depths. Furthermore, as the depth increases, the uniaxial compressive strength of rocks tends to rise.  
 206 Nevertheless, to simplify the description of methods, we have chosen to disregard the influence of depth  
 207 on the uniaxial compressive strength of granite rock.

208 **Table 3.** Computed piezoelectric and elastic energy parameters for a granite block with each side of 40 m, along  
 209 with the Richter magnitude ( $M_L$ ) of the incoming earthquake

Time, days	Detected photons' Energy, MeV	$E_e$ , MeV	Voltage, V	$F$ , N	$\sigma$ , MPa	$E_{el}$ , joule	$M_L$
1	0.0001	25.60	25601074	64734145014	40.45	2619068457	3.39
10	0.001	25.64	25645482	64846433182	40.52	2628162435	3.39
100	0.01	26.09	26093818	65980083460	41.23	2720857133	3.40
200	0.1	31.03	31031681	78465823145	49.04	3848053376	3.48
350	0.2	37.62	37621495	95128639253	59.45	5655911254	3.58
500	0.4	55.29	55296489	1.39821E+11	87.38	12218716382	3.77
700	0.5	67.03	67039120	1.69513E+11	105.94	17959203977	3.87

210  
 211 Based on the information presented in Table 2 and depicted in Fig. 1, the graph showcases the relationship  
 212 between the calculated uniaxial compressive stress applied on a granite block, measuring 40 m on each  
 213 side, and the corresponding recording day of the particles' energy. The graph suggests that a logarithmic  
 214 function provides a better fit for the data. Assuming the uniaxial compressive strength of the granite rock  
 215 is 140 MPa, it can be inferred that approximately on the 870th day, this block would experience rupture  
 216 due to the uniaxial compressive stress. Consequently, an earthquake with a magnitude of approximately 4  
 217 on the Richter scale is expected to occur.





218

219 **Fig.1. Relationship between the calculated uniaxial compressive stress ( $\sigma$ ) applied on a granite block with each side**  
 220 **of 40 m and the recording time of the particles' energy. Logarithmic extrapolation was shown with a dashed line.**

221

222 In the analysis mentioned above, a constant dimension was assumed for granite blocks (each side measuring  
 223 40 m) to determine the quantities of uniaxial mechanical stress. However, with the increase in elastic energy  
 224 within the Earth's crust, the area affected by mechanical stress that could potentially rupture also increases  
 225 (Mohajer-Ashjaei & Noroozi (1978)). If we were to consider a larger size for the granite block, such as 80

226

227 m for each side, the applied uniaxial stress ( $\sigma$ ) would be half of the previous amount, resulting in double  
 228 the elastic energy due to the applied stress and higher  $M_L$  quantities, as shown in Table 4. Consequently,  
 229 the occurrence of an earthquake would be delayed to the 1320th day instead of the 870th day as illustrated

230

231 in Fig. 2. Therefore, this method is only applicable when the size of the block affected by uniaxial  
 232 compressive stress is known. The size of the block may be approximated using deep underground particle

233

234 detectors or stress sensors spread across an area, enabling the creation of a 3D contour map illustrating the  
 235 energies of detected particles or the amount of accumulated stress over time. The areas with high particle

236

237 flux/energies experience greater stress, while areas with zero particle flux/energies are not affected by the  
 238 underground stress. Through this approach, an approximate estimation of the block size can be derived. If

239

240 this size is constant over time, it will be possible to apply the above-mentioned technique to predict the time  
 of earthquake occurrence.

237

238 In addition, if there is already a fault in that block, one should first calculate the shear stress in the fault  
 239 based on the amount of uniaxial compressive stress calculated according to the energy of the detected

240

241 particles. Subsequently, by comparing this value with the shear strength of the fault-filling material, one  
 can estimate the timing of a potential earthquake occurrence. Within the depth of 0-10 km, the average

241 shear strength of fault gouge along the fault surface is approximately equal to or less than 10 MPa (Kunquan  
 242 et al. (2018)).

243

244

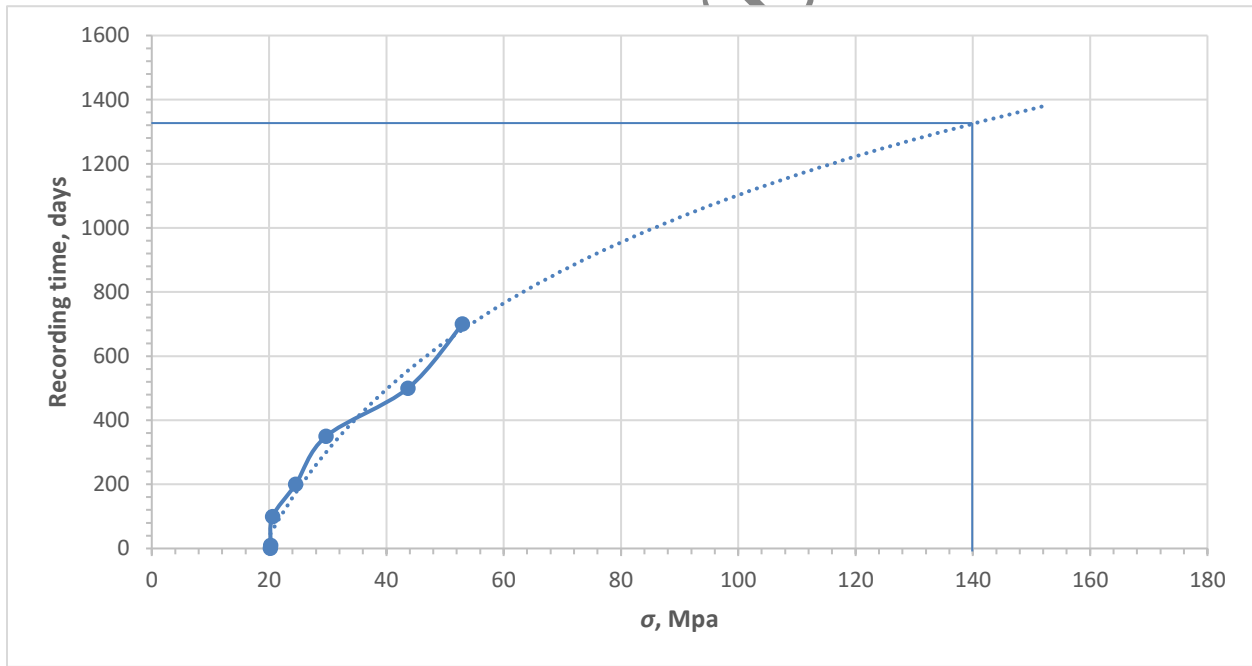
245

246

**Table 4.** Computed piezoelectric and elastic energy parameters for a granite block with each side of 80 m, along with the Richter magnitude ( $M_L$ ) of the incoming earthquake

Time, days	Detected photons' Energy, MeV	$E_e$ , MeV	Voltage, V	$F$ , N	$\sigma$ , MPa	$E_{el}$ , joule	$M_L$
1	0.0001	25.60	25601074	1.29E+11	20.2	2619068457	3.56
10	0.001	25.60	25645482	1.29E+11	20.2	2628162435	3.56
100	0.01	26.09	2609381	1.31E+11	20.6	2720857133	3.57
200	0.1	31.00	31031681	1.56E+11	24.5	3848053376	3.65
350	0.2	37.60	37621495	1.90E+11	29.7	5655911254	3.75
500	0.4	55.29	55296489	2.79E+11	43.7	12218716382	3.94
700	0.5	67.03	67039120	3.3E+11	52.9	17959203977	4.04

247



248

**Fig.2.** Relationship between the calculated uniaxial compressive stress ( $\sigma$ ) applied on a granite block with each side of 80 m and the recording time of the particles' energy. Logarithmic extrapolation was shown with a dashed line.

251

252

253

Another method is considering if the piezoelectric rock with a variable size is fractured on a specific day, how much energy is released. Within this approach, we will not predict when the earthquake will happen,

254 rather, we will estimate how much stored energy will be released if an earthquake happens on a particular  
 255 day.

256 Upon obtaining data on the energy of detected particles, the energy of electrons ( $E_e$ ) and the voltage  
 257 produced ( $V$ ) by the piezoelectric rocks can be calculated using Eq. 10 and Eqs. 11-15, respectively.  
 258 Subsequently, Eq. 15 can be utilized to determine the value of  $F/x$ . By assuming that the final uniaxial  
 259 compressive stress applied to the block would cause it to break and trigger an earthquake on that day (due  
 260 to the elastic energy stress surpassing the final uniaxial strength of the block; i.e.,  $\sigma = F/x^2 = 140$  MPa), the  
 261 size of the block (parameter  $x$  for each side) can be estimated. Through the computation of the force ( $F$ ),  
 262 the amount of elastic energy ( $E_{el}$ ) released on that specific day can be evaluated.

263 The outcomes of this methodology for the provided data are presented in Table 5. As indicated in the table,  
 264 for a granite block with a piezoelectric coefficient of  $7 \times 10^{-13}$  C/N, uniaxial compressive strength of 140  
 265 MPa, and elastic modulus of 40 GPa, over a 700-day period, the values of  $V$ ,  $F$ ,  $E_{el}$ ,  $x$ , and  $M_L$  increase as  
 266 the energy of detected photons rises. On the 700th day, the detected photons' energy suggests that if an  
 267 earthquake were to occur on that day, a cubic granite block with a volume of  $30.27^3$  m<sup>3</sup> would rupture,  
 268 releasing elastic energy amounting to  $6.7 \times 10^9$  J and resulting in an earthquake with a magnitude of  
 269 approximately 3.8 on the Richter scale.

270

271 **Table 5.** Computed piezoelectric and elastic energy parameters for a granite block with variable size, along with the  
 272 Richter magnitude ( $M_L$ ) of the incoming earthquake

Time, days	The energy of crossing photons, MeV	$E_e$ , MeV	Voltage, V	$F$ , N	$\sigma$ , MPa	$x$ , m	$E_{el}$ , joule	$M_L$
1.00	0.0001	25.6	25601074	18707631833	140	11.56	378444547	3.09
10.00	0.001	25.6	25645482	18772588823	140	11.58	380417320	3.09
100.00	0.01	26.0	26093818	19434693809	140	11.78	400719599	3.10
200.00	0.1	31.0	31031681	27486095543	140	14.01	673974722	3.23
350.00	0.2	37.6	37621495	40399366098	140	16.99	1200980226	3.37
500.00	0.4	55.3	55296489	87276545588	140	24.97	3813470170	3.66
700.00	0.5	67.0	67039120	128280028403	140	30.27	6795362073	3.80

273

274 It is important to acknowledge that the aforementioned analyses for earthquake prediction assume a  
 275 constant uniaxial compressive strength and constant piezoelectric and dielectric coefficients for granitic  
 276 rocks. However, it should be noted that these parameters may vary for different types of rocks. Additionally,  
 277 the mechanism of stress that affects the Earth's crust, such as shear or tension stress, tri-axial stress, etc.,

278 may differ as well. Furthermore, as the depth increases, the piezoelectric coefficient decreases due to rising  
279 temperatures. Consequently, the results obtained from both analyses will inevitably be approximate.

280 It should be considered that there are many reports of earthquake precursors in the scientific literature, of  
281 about twenty different types that range from meteorology to zoology, and so far none of them have been  
282 completely reliable for earthquake prediction. However, our study introduces methods to estimate the time  
283 or energy of an impending earthquake, based on the detected particle energy. These methods can have  
284 appropriate reliability compared to other methods, because from our previous study, using elastic energy  
285 and piezoelectric formulas and applying Monte Carlo simulation, we know that there is a relationship  
286 between the increase in the energy of radiated atomic/nuclear particles and the elastic energy, stored in a  
287 granite block. Since granite rocks make up approximately 60% of the Earth's crust, the increase in the  
288 energy of the detected particles in a certain period of time can be considered as an important precursor for  
289 the impending shallow earthquake.

290 Besides, to enhance the accuracy of these methods, it would be advantageous to drill deep holes around  
291 faults and install long-term or permanent logging detectors downhole, close to the earthquake hypocenter,  
292 to monitor and detect the radiated particles with their initial energies. This proposal is completely  
293 operational and has already been implemented in projects such as SAFOD (San Andreas Fault Observatory  
294 at Depth) in the United States in a period of time and useful information was obtained from the behavior of  
295 the San Andreas fault (Zoback et al. (2011)).

296

#### 297 4. Conclusion

298 This study has introduced methods to estimate the time/ energy of earthquakes in aseismic regions by  
299 measuring the energy of radiated particles from underground piezoelectric rocks using particle detectors on  
300 the surface or downhole. As the energy of the detected particles rises, the stored elastic energy of the granite  
301 block also increases, potentially reaching a critical rupture point, at which point this energy is released  
302 suddenly, leading to the occurrence of an earthquake.

303 It should be mentioned that the most detected particles are likely to pass through vacuum-filled or  
304 lightweight fluid-filled fractures and reach the detectors.

305 Furthermore, it is important to note that the introduced methods are approximate estimations, as they  
306 assume constant parameters for the piezoelectric rock. In addition, we have supposed the earthquake  
307 happened in a piezoelectric block. If the earthquake does not occur in such types of rocks and does not emit  
308 any atomic or nuclear particles, it cannot be predicted using the mentioned approaches.

309 Continued research into particles' radiation anomalies and their potential role in earthquake prediction  
310 could contribute to our understanding of these complex natural phenomena in the future.

311

#### 312 **Data availability statement**

313 The data that support the findings of this study are available from the corresponding author upon reasonable  
314 request

315

#### 316 **Funding and/or Conflicts of interests/Competing interests**

317 There is no funding for this research.

318 There are no conflicts of interest for this research.

319

320

#### 321 **5. References**

322 Bahari, A., Mohammadi S., Shakib N. S., Benam M. R., Sajjadi,Z. (2024), Monte Carlo Methods to  
323 Simulate the Propagation of the Created Atomic/ Nuclear Particles from Underground Piezoelectric  
324 Rocks through the Fractures Before the Earthquakes, Atom Indonesia, Volume: 50, Number: 1, Pages:  
325 27-35, DOI: 10.55981/aij.2024.1311

326 Bahari, A., Mohammadi S. (2024), Simulating the Interactions between the Produced Neutrons from  
327 Piezoelectric Rocks and the Surrounded Medium during the Earthquakes, Accepted for publication in  
328 Iranian Journal of Physics Research.

329 Bahari A. Mohammadi S., Benam M. R., Sajjadi,Z. (2022), Simulation with Monte Carlo Methods to Find  
330 Relationships between Accumulated Mechanical Energy and Atomic/Nuclear Radiation in  
331 Piezoelectric Rocks with Focus on Earthquakes, Radiation effects and defects in solids, Volume: 177,  
332 Issue: 7-8, Pages: 743-767, DOI: 10.1080/10420150.2022.2073885.

333 Borla O., Lacidogna G., and Carpinteri A. (2015), Chapter: Piezonuclear neutron emissions from  
334 earthquakes and volcanic eruptions, Book: *Acoustic, Electromagnetic, Neutron Emissions from  
335 Fracture and Earthquakes* (by Carpinteri A. et al.), Publisher: Springer International Publishing  
336 Switzerland.

337 Finkelstein D. and Powell J., Earthquake lightning (1970), Nature, Volume: 228, Pages: 759.

338 Fu C. C., Wang P. K., Lee L. C., Lin C. H., Chang W. Y., Giuliani G., Ouzounov D. (2015), Temporal  
339 variation of gamma rays as a possible precursor of earthquake in the Longitudinal Valley of eastern  
340 Taiwan, *Journal of Asian Earth Sciences*, Volume: 114, Issue: 2, Pages: 362. DOI:  
341 10.1016/j.jseaes.2015.04.035.

342 Gao L., Gao F., Xing Y., Zhang Z. (2020), An Energy Preservation Index for Evaluating the Rockburst  
343 Potential Based on Energy Evolution, *Energies*, Volume: 13, Issue: 14, Pages: 3636. DOI:  
344 10.3390/en13143636

345 Gutenberg B. and Richter C. F. (1956), Earthquake magnitude, intensity, energy, and acceleration (Second  
346 paper), *Bulletin of the Seismological Society of America*, Volume: 46, Issue: 2, Pages: 105-145.

347 Hadfield R.H. (2009), Single-photon detectors for optical quantum information applications, *Nature*  
348 *Photonics* Volume: 3, Issue: 12, Pages: 696-705.

349 Halliday D., Resnick R. (1974), *Fundamentals of Physics*, Publisher: Wiley, New York.

350 Hubbard S. S., Peterson J. E., Majer E. L., Zawislanski P. T., Williams K. H., Roberts J., Wobber F. (1997),  
351 Estimation of permeable pathways and water content using tomographic radar data, *The Leading Edge*,  
352 Volume: 16, Issue: 11, Pages: 1623-1628.

353 Kunquan L., Zexian C., Meiying H., Zehui J., Rong S., Qiang W., Gang S. Jixing L., (2018), The  
354 mechanism of earthquake, *International Journal of Modern Physics B*, Volume: 32, Pages: 1850080.

355 Liang C. Wu S., Li X., Xin P. (2015), Effects of strain rate on fracture characteristics and mesoscopic failure  
356 mechanisms of granite, *Int. J. Rock Mech. And Min. Sci.*, Volume: 76, Pages: 146-154.

357 Maksudov A. U., Zufarov M. A. (2017), Measurement of neutron and charged particle fluxes toward  
358 earthquake prediction, *Earthquake Sci.*, Volume: 30, Issue: 5-6, Pages: 283.

359 Mansouri Daneshvar M.R. and Freund F.T. (2019), Examination of a relationship between atmospheric  
360 blocking and seismic events in the Middle East using a new seismo-climatic index *Swiss J.*  
361 *Geosci.* Volume:112, Pages: 435-451.

362 Matsuda T., Yamanaka C., Ikeya M. (2005), Piezoelectric Measurements of Granite as Composite Material  
363 Using Atomic Force Microscope, *Japanese Journal of Applied Physics*, Volume: 44, Issue: 2, Pages:  
364 968-971.

365 Moheimani R. S. O., Fleming A. J. (2006), *Piezoelectric Transducers for Vibration Control and Damping*,  
366 Chapter: *Fundamentals of Piezoelectricity*, Springer London, Pages: 9-35.

367 Mohajer-Ashjai A. and Nowroozi A. A. (1978), Observed and probable intensity zoning of Iran,  
368 Tectonophysics, Volume: 49, Issues: 3–4, Pages: 149-160, DOI: 10.1016/0040-1951(78)90173-7.

369 National Institute of Standards and Technology (NIST), High Efficiency in the Fastest Single-Photon  
370 Detector System (Press release), 2013, Retrieved 2018-10-11.

371 Sigaeva E., Nechaev O., Panasyuk M., Bruns A., Vladimirsky B. and Kuzmin Y. (2006), Thermal neutrons'  
372 observations before the Sumatra earthquake, Geophys. Res. Abstr., Volume: 8, Pages: 00435.

373 Volodichev N. N. Kuzhevskij B.M., Nechaev O.Y., Panasyuk M.I., Podorolsky A.N., Shavrin P.I. (2000),  
374 Sun-Moon-Earth connections: the neutron intensity splashes and seismic activity, Astron. Vestnik,  
375 Volume: 34, Pages: 188.

376 Zoback, M. D., S. Hickman, W. Ellsworth, and the SAFOD Science Team (2011), Scientific drilling into  
377 the San Andreas Fault Zone—An overview of SAFOD's first five years, Sci. Drill., Volume: 11,  
378 Pages: 14-28, DOI:10.2204/iodp.sd.11.02.2011.

379

Article in Press (Unedited)